A mechanistic model for compaction of granular aggregates moderated by pressure solution

Hideaki Yasuhara, Derek Elsworth, and Amir Polak

Department of Energy and Geo-Environmental Engineering, Pennsylvania State University, University Park, Pennsylvania, USA

[1]   A model is presented for the compaction of granular aggregates that accommodates the serial processes of grain-contact dissolution, grain-boundary diffusion, and precipitation at the pore wall. The progress of compaction and the evolution of the mass concentration of the pore fluids may be followed with time, for arbitrary mean stress, fluid pressure, and temperature conditions, for hydraulically open or closed systems, and accommodating arbitrary switching in dominant processes, from dissolution, to diffusion, to precipitation. Hindcast comparisons for compaction of quartz sands [*Elias and Hajash*, 1992] show excellent agreement for rates of change of porosity, the asymptotic long-term porosity, and for the development of silica concentrations in the pore fluid with time. Predictions may be extended to hydraulically open systems where flushing by meteoric fluids affects the compaction response. For basins at depths to a few kilometers, at effective stresses of 35 MPa, and temperatures in the range 75°–300°C, rates of porosity reduction and ultimate magnitudes of porosity reduction increase with increased temperature. Ultimate porosities asymptote to the order of 15% (300°C) to 25% (75°C) at the completion of dissolution-mediated compaction and durations are accelerated from a few centuries to a fraction of a year as the temperature is increased. Where the system is hydraulically open, flushing elevates the final porosity, has little effect on evolving strain in these precipitation-controlled systems, and depresses pore fluid concentrations. These effects are greatest at lower temperatures.   *INDEX TERMS:* 5120 Physical Properties of Rocks: Plasticity, diffusion, and creep; 5139 Physical Properties of Rocks: Transport properties; 8045 Structural Geology: Role of fluids; 8160 Tectonophysics: Evolution of the Earth: Rheology—general; *KEYWORDS:* compaction, pressure solution, permeability, dissolution, precipitation, basin mechanics

1.   Introduction

[2]   The compaction and concurrent cementation of granular aggregates is observed to be controlled by the rates of grain-contact crushing, grain-contact interpenetration, and the redistribution of mobilized mass from these contacts. Together, these processes control the rate of porosity loss and the evolution of strength with time. One of the main mechanisms of diagenetic compaction and deformation in sedimentary rocks is pressure solution, which has been studied in some detail [e.g., *Weyl*, 1959; *Robin*, 1978; *Rutter*, 1976; *Renard et al.*, 1997]. Pressure solution involves three linked processes: dissolution at the stressed interfaces of grain-to-grain contacts, diffusive transport of dissolved matter from the interface to the pore space, and finally, precipitation at the less-stressed surface of the grains. For stress-induced dissolution, two mechanisms have been proposed. One is water film diffusion (WFD), which involves dissolution in grain-to-grain contacts where stresses are concentrated, followed by

the subsequent diffusion of matter through an absorbed interfacial fluid film into the pore fluid [*Weyl*, 1959; *Coble*, 1963; *Rutter*, 1976; *Raj*, 1982]. The other is plastic deformation plus free-face pressure solution (PD + FFPS), which involves dissolution from the edges of grain-to-grain contacts into the pore fluid and may result in undercutting of the contacts [*Engelder*, 1981; *Tada and Siever*, 1986; *Tada et al.*, 1987]. Both these mechanisms are plausible, although no established evidence is available that identifies either WFD or PD + FFPS as the unique mechanism to explain pressure solution creep. Rather, these twin mechanisms are likely to contribute in varying degrees to the observed response, with the dominant control asserted by particular conditions of stress, temperature, and mass transport conditions at the grain contacts and in the pore fluids.

[3]   The parameters exerting control over these complementary mechanisms of mass redistribution remain poorly defined. A variety of models have been proposed to describe deformation or compaction of porous aggregates associated with pressure solution. These models can be classified into two main types. In the first set, a viscous law [e.g., *Rutter*, 1976; *Raj*, 1982; *Dewers and Ortoleva*, 1990; *Dewers and*

Hajash, 1995] is utilized to match laboratory experiments, which are generally conducted over a relatively short period, on the order of hundreds of days. These models take into account the chemistry of the minerals and pore fluids (i.e., dissolution and precipitation) and the transport of dissolved matter (i.e., diffusion). However, their extrapolation to geological timescales is difficult as the experiments do not attain long-term equilibrium. In the second set of models, a purely plastic law is applied to interpret equilibrium compaction phenomena [*Palciauskas and Domenico*, 1996; *Stephenson et al.*, 1992]. Such models are developed from simple energy and volume balance considerations and quantitatively describe the compaction of porous aggregates in terms of their applied stress and temperature history.

[4] These two complementary models, involving viscous and plastic flow laws may predict the change in porosity with time for isothermal creep experiments and natural compaction in sedimentary basins, respectively. However, to obtain a consistent prediction of the diminution in porosity over a range of short to long timescales, the attributes of the short-term (viscous) and long-term (plastic) behaviors must be combined. Poroviscoplastic models [*Lehner*, 1995; *Revil*, 1999, 2001] are able to accommodate these two end-member responses, where the progress of transient compaction to an equilibrium state is followed. These models describe piston-like interpenetration of grains under assumed time-invariant geometry and require the selection of a dominant compaction mechanism a priori. Although able to match compaction data over various timescales, the omission of the role of precipitation and of the mass carried in the pore fluid restricts a more mechanistic description of the interpenetration process. An alternative to using lumped parameter models to represent the viscous compaction process is to adopt mechanistic models that rigorously accommodate the mechanisms of dissolution, transport, and precipitation. This is the approach taken here to follow the micromechanical processes that control compaction behavior. Resulting changes in grain geometry are explicitly followed, as interpenetration proceeds, enabling, for the first time, rates of compaction, the role of precipitation, and their resulting influence on the evolution of permeability to be followed.

[5] The observation that sandstones of vastly different ages retain significant porosity requires that some process must halt the pressure-solution-mediated redistribution of cementation at late times. In this work we follow the stress- and temperature-dependent controls on compaction where porosity loss is controlled by the evolving interpenetration of the grains comprising the aggregate. Interpenetration is mediated by rates of dissolution at grain-to-grain contacts, by the transport of this aqueous solution along the grain-to-grain contact to the pore fluid reservoir, and from there to a final precipitation site on the exposed pore wall. Importantly, the controlling influence of grain-boundary dissolution, of grain-boundary diffusion, and of precipitation to the pore wall evolves naturally in time, enabling both ultimate porosity and the evolving pore fluid concentration to be correctly accommodated.

2. Conceptual Model

[6] In this work a mechanistic model is presented to describe the compaction of porous aggregates that incorpo-
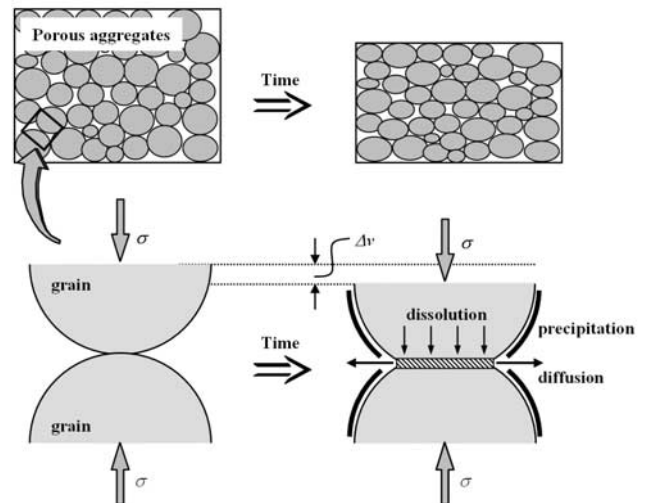

Figure 1. Schematic of pressure solution. At grain-to-grain contacts, the mineral dissolves due to the high stress concentration. Solutes diffuse from the interface into the pore space. Finally, precipitation occurs as a result of oversaturation of solutes in the pore fluid.

rates the important effects of grain interpenetration that accompany the redistribution of mass by pressure solution. The model comprises three important, but physically justified, components. The first is a control on the asymptotic reduction in porosity of the aggregate, controlled by an interaction between the surface energy of the quartz grains and the reduction in the grain-to-grain stress state occasioned by grain interpenetration. The second is a control on the rate of compaction that results from mass redistribution from the grain contacts to the pore walls; this is through the serial processes of dissolution at the grain interfaces, diffusive transport along the grain boundaries, and finally by precipitation on free faces, as illustrated schematically in Figure 1. Finally, mass transfer from the grain contacts to the pore walls irreversibly modifies the geometry of the aggregate and the interconnectedness of the pore space. The reduction in contact stresses that accompanies the interpenetration of the grain contacts provides a reinforcing feedback in slowing the rate of porosity reduction by reducing dissolution rates and by concurrently increasing diffusion pathways lengths. The interaction of these three mechanisms enables the decaying rate of porosity reduction to be followed from a mechanistic standpoint and the evolution of quartz concentrations in the pore fluids to be followed.

2.1. Equilibrium Behavior

[7] Where hydrostatic stress is applied to a porous aggregate, grain interpenetration will develop as a result of high localized contact stresses. Transient interpenetration may develop by plastic creep as the intergranular stress remains in excess of a critical stress, σ_c. Where stresses remain in excess of the critical interpenetration stress, dissolution will develop in the water film enveloping the interface, and mass will be transported by dissolution. This transport will be accompanied by an increase in contact area, which will continue until stresses acting on grain-to-grain contacts

reach the critical stress σ_c. This process will continue until the applied contact stress is sufficiently reduced by the growth of the contact area that compaction essentially ceases. The limiting stress may be determined from the consideration of energy balance under applied stress and temperature conditions. The critical stress σ_c may be defined as [*Revil*, 1999; modified from *Stephenson et al.*, 1992]

$$\sigma_c = \frac{E_m(1 - T/T_m)}{4V_m}, \tag{1}$$

where E_m and T_m are the heat and temperature of fusion, respectively. V_m is molar volume of the solid. (E_m = 8.57 kJ mol^{-1}, T_m = 1883 K, and V_m = 2.27 × 10^{-5} m^3 mol^{-1} for quartz). This critical stress σ_c defines the stress state where the compaction of the aggregate will effectively halt.

2.2. Rates of Dissolution

[8] Mass redistribution in compacting aggregates is controlled by the serial processes of dissolution, diffusion along the interfacial water film, and then by precipitation from the pore fluid to the pore wall. Dissolution creep controls the first of these serial processes through stress-mediated dissolution at grain-to-grain contacts. Dissolution at the grain contacts provides a source of mass that may be redistributed by diffusion along an intergranular water layer. The rate of compaction is influenced both by the absolute rate of mass diffusion along this interface and by the lengthening of the diffusion path as the grains interpenetrate and the contact area grows. The strain rate at the grain boundary may be defined as [*Revil*, 1999; modified from *Raj*, 1982]

$$\dot{\varepsilon}_{\text{diss}} = \frac{3V_m k_+}{RTd}(-\Delta\mu), \tag{2}$$

where $\dot{\varepsilon}_{\text{diss}}$ is the strain rate, V_m is the molar volume of quartz, k_+ is the dissolution rate constant of quartz, which can be obtained by experimental results [*Rimstidt and Barnes*, 1980; *Dove and Crerar*, 1990], R is the gas constant, T is the temperature of the system, and d is the grain diameter. In this equation, $\Delta\mu$ represents the chemical potential difference between the compressive site of the grain-to-grain contact and the less-stressed site of the pore wall and is the motive force driving pressure solution (the negative sign is expressed because of the thermodynamic convention; $\Delta\mu = \mu_{\text{last}} - \mu_{\text{initial}}$). Applying nonhydrostatic and nonequilibrium thermodynamics, the chemical potential at the stressed grain-to-grain contact, μ, is defined as [*Heidug*, 1995].

$$\mu = (\sigma_a + p)V_m + f - 2H\gamma V_m, \tag{3}$$

where σ_a is the disjoining pressure [e.g., *Tada et al.*, 1987] equal to the amount by which the pressure acting at the grain-to-grain contacts exceeds the hydrostatic pore pressure, p is the pore pressure, and f is the molar Helmholtz free energy which may consist of elastic and plastic strain energy. The last term on the right-hand side represents a surface energy at the grain-to-grain contact, where H is the mean local curvature of the solid-fluid interface, and γ is the specific interfacial energy at the grain-to-grain contact. Since pressure acting on the free face of the grains is the

hydrostatic pore pressure, the chemical potential difference, $\Delta\mu$, for the solute is given by

$$-\Delta\mu = \sigma_a V_m + \Delta f - 2H\gamma V_m, \tag{4}$$

where Δf is the molar Helmholtz free energy difference between the stressed grain-to-grain contacts and the free pore walls.

[9] For simplicity, in a uniaxial compressive condition of two grains that are subject to nonhydrostatic stress and assuming that the stress applied at the contact area does not vary with the location in the interface, the disjoining pressure, σ_a, is given by

$$\sigma_a = \frac{\sigma_{\text{eff}}}{\varphi}, \tag{5}$$

where σ_{eff} is the effective stress, defined as the average stress acting on the grains exceeding the pore pressure, and φ ($0 < \varphi < 1$) is the ratio of the contact area to the maximum cross-sectional area normal to the applied stress. When the system reaches thermodynamic equilibrium, the chemical potential difference will be zero, and stress applied at the grain contact area, σ_a, will reach the critical stress, σ_c, which is defined in equation (1). Therefore from equations (4) and (5) these yield at equilibrium

$$\sigma_a^{\text{eq}} = \sigma_c = \frac{\sigma_{\text{eff}}}{\varphi^{\text{eq}}} = 2\gamma H^{\text{eq}} - \frac{\Delta f^{\text{eq}}}{V_m}, \tag{6}$$

where the superscript *eq* denotes the equilibrium condition for each term. Substituting equation (6) into the chemical potential relation of equation (4) yields

$$-\Delta\mu \approx (\sigma_a - \sigma_c)V_m, \tag{7}$$

and provides a threshold stress, σ_c, for the initiation of pressure solution. Substituting this into equation (2), the compaction strain rate through dissolution at grain-to-grain contacts is given by

$$\dot{\varepsilon}_{\text{diss}} = \frac{3V_m^2 k_+}{RTd}(\sigma_a - \sigma_c). \tag{8}$$

[10] In the literature the chemical potential difference is defined as $-\Delta\mu = \sigma_{\text{eff}}V_m$ [e.g., *Shimizu*, 1995; *Paterson*, 1995] by adopting the effective stress, σ_{eff}, instead of the disjoining pressure, σ_a, and by neglecting the effects of the strain energy term, Δf, and the surface energy term, $2H\gamma V_m$. Substituting this chemical potential difference into equation (2), the compaction strain rate is given by

$$\dot{\varepsilon}_{\text{diss}} = \frac{3V_m^2 k_+}{RTd}\sigma_{\text{eff}}. \tag{9}$$

[11] This expression of equation (9) is equivalent to that proposed by *Raj* [1982] (modified by *Revil* [1999]) and *Shimizu* [1995]. In this expression, however, the stress acting on the contact area, which may be much larger than the effective stress due to stress localization, and the equilibrium condition are not taken into account.

[12] The appropriateness of a critical stress where pressure solution ceases (i.e., the validity of equation (8)), is supported by experimental data. Table 1 and Figure 2 show

Table 1. Comparison of Compaction Rates Through Dissolution[a]

	Strain Rates Through Dissolution $\dot{\varepsilon}_{\mathrm{diss}}$, s^{-1}		
	Experiment[b]	Equation (8)	Equation (9)
Elias and Hajash [1992]; *150°C, d = 110 μm*			
σ_{eff} = 17.2 Mpa	2.65×10^{-9}	1.29×10^{-8}	1.05×10^{-10}
σ_{eff} = 34.96 Mpa	7.26×10^{-9}	1.63×10^{-8}	2.11×10^{-10}
σ_{eff} = 69.9 Mpa	2.84×10^{-8}	2.07×10^{-8}	4.23×10^{-9}
Dewers and Hajash [1995]; σ_{eff} = 34.5 MPa			
150°C, d = 110 μm	4.00×10^{-8}	2.67×10^{-8}	3.46×10^{-10}
150°C, d = 210 μm	1.00×10^{-8}	1.40×10^{-8}	1.81×10^{-10}
200°C, d = 210 μm	8.30×10^{-8}	1.04×10^{-7}	1.35×10^{-9}

[a]Here $k_+ = 2.51 \times 10^{-9}$ and 2.14×10^{-8} mol m^{-2} s^{-1}, and σ_c = 73.2 and 70.7 MPa at 150° and 200°C, respectively. Equations to obtain these values are given in text. Here $\sigma_a = 2.18 \times 10^3$, 2.74×10^3, and 3.45×10^3 MPa at σ_{eff} = 17.2, 34.96, and 69.9 MPa, respectively.

[b]For the experiments of *Elias and Hajash* [1992], the strain rates are calculated using the equation of $\dot{\varepsilon}_{\mathrm{diss}} = d[\phi(t) - \phi_0]/dt(1 - \phi_0)^{-1}$, where $\phi(t)$ and ϕ_0 are porosities at a given time, t, and at $t = 0$, respectively. Changes in porosity with time are obtained from their Figure 4. For the experiments of *Dewers and Hajash* [1995], the strain rates are obtained from their Table 2.

a comparison of dissolution-driven strain rates measured in closed-system experiments [*Elias and Hajash*, 1992; *Dewers and Hajash*, 1995] (the experimental results may also incorporate the unquantified contribution of dissolution kinetics in contributing to the observed strain rates) and their correspondence with rates from relations of the form of equations (8) and (9). In equation (8) the stresses acting on the grain contact area, σ_a, are assumed to be the average stresses acting on the Hertzian contacts, which would be a reasonable approximation at an early time in the compaction process. As is apparent in Figure 2, behavior is better represented by the consideration of a limiting stress (equation (8)) rather than absolute stress magnitude (equation (9)). The latter underpredicts rates by about two orders of magnitude.

[13] In defining mass redistribution, it is sometimes convenient to relate dissolution mass fluxes, dM_{diss}/dt, to strain rates. The strain rate, $\dot{\varepsilon}_{\mathrm{diss}}$ is expressed as $\dot{\varepsilon}_{\mathrm{diss}} = (1/V)dV/dt$ where V is the bulk volume, and in the one-dimensional case it is approximated as

$$\dot{\varepsilon}_{\mathrm{diss}} \approx \frac{1}{d}\frac{\Delta d}{\Delta t}, \quad (10)$$

where d is grain diameter, and using the dissolution mass flux, dM_{diss}/dt, $\Delta d/\Delta t$ is expressed as

$$\frac{\Delta d}{\Delta t} \approx \frac{dM_{\mathrm{diss}}}{dt}\frac{1}{\rho_g}\frac{1}{(\pi/4)d_c^2}, \quad (11)$$

where ρ_g is the grain density (2650 kg m^{-3} for quartz), d_c is the diameter of the grain-to-grain contacts, and the term $\pi/4d_c^2$ represents the contact area at the interface. From equations (8), (10), and (11), the dissolution mass flux, dM_{diss}/dt, is then given by

$$\frac{dM_{\mathrm{diss}}}{dt} = \frac{3\pi V_m^2(\sigma_a - \sigma_c)k_+\rho_g d_c^2}{4RT}. \quad (12)$$

2.3. Rates of Diffusion

[14] Once transferred into solution, mass is transported from the grain contact to the pore fluid, via diffusion. The diffusion of solute under steady state conditions is described by Fick's first law

$$J = -D_b\frac{dC}{dx}, \quad (13)$$

where J is the flux of solute, D_b is the diffusion coefficient, and dC/dx is the concentration gradient. On the basis of equation (13), the diffusive mass flux, J_m, from a circular contact of radius r is given by

$$J_m = -2\pi r\omega D_b\left(\frac{dC}{dx}\right)_{x=r}, \quad (14)$$

where ω is the thickness of the water film trapped at the interface, and the term $2\pi r\omega$ represents the area through which that solution diffuses when $x = r$. Integrating equation (14) in the range $a \leq x \leq d_c/2$ the diffusive mass flux, the rate of removal of solute from the interface and into the pore space, is defined as

$$J_m = \frac{dM_{\mathrm{diff}}}{dt} = \frac{2\pi\omega D_b}{\ln(d_c/2a)}(C_{\mathrm{int}} - C_{\mathrm{pore}}), \quad (15)$$

where dM_{diff}/dt is the diffusive mass flux, and $(C_{\mathrm{int}})_{x=a}$ and $(C_{\mathrm{pore}})_{x=d_c/2}$ are concentrations in the interface and pore space, respectively.

2.4. Rates of Precipitation

[15] Mass removed from the interface and delivered to the adjoining pore fluid is available to precipitate on the exposed pore wall. Precipitation of the solute to the free faces of the pore wall is described using the precipitation rate constant of quartz [*Canals and Meunier*, 1995; *Renard et al.*, 1997]

$$\frac{dC_{\mathrm{pore}}}{dt} = \frac{A}{M}k_-(C_{\mathrm{pore}} - C_{\mathrm{eq}}), \quad (16)$$

where A is the relative grain surface area, and M is the relative mass of the fluid, which are the dimensionless
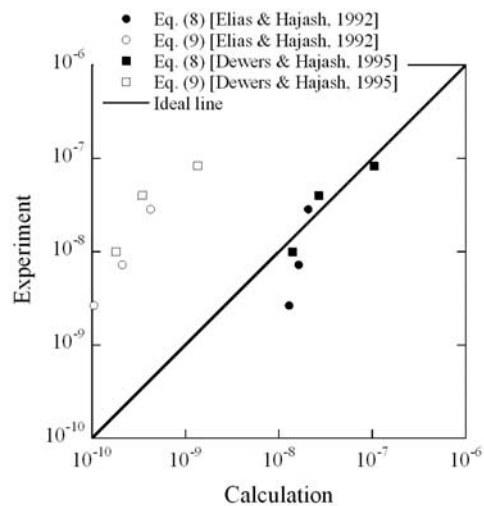

Figure 2. Comparison of observed compactive strain rates, resulting from dissolution [*Elias and Hajash*, 1992; *Dewers and Hajash*, 1995] with calculations assuming a critical stress at which pressure solution ceases (equation (8)), and absent this critical stress (equation (9)).

parameters defined by *Rimstidt and Barnes* [1980]. C_{pore} is the concentration of solute in the pore fluid, k_- is the precipitation rate constant of quartz, available from laboratory studies [*Rimstidt and Barnes*, 1980; *Bird et al.*, 1986], and C_{eq} is the solubility of quartz [*Fournier and Potter*, 1982; *Ragnarsdóttir and Walther*, 1983].

[16] The precipitation mass flux, the rate of deposition of solute from the pore space onto the grain surfaces, is defined by

$$\frac{dM_{prec}}{dt} = V_p \frac{A}{M} k_- \left(C_{pore} - C_{eq} \right), \qquad (17)$$

where dM_{prec}/dt is the precipitation mass flux, and V_p is the volume of pore space.

2.5. Geometric Modification by Grain Interpenetration

[17] Mass flux rates, and thereby rates of compactive strain of the aggregate, are controlled by the interaction of dissolution, diffusion, and precipitation processes. These mass redistribution processes irreversibly alter the shape of the aggregate and, in particular, the form of the intergranular contacts. We assume an initial face-centered cubic aggregate of uniformly sized contacting spheres, fully saturated by water. More realistic packing arrangements can be considered, but uncertainties in details of these packing geometries, including the number of contacts per grain when compaction proceeds, do not justify its attempt. Initially, the system is treated as a closed system, with the representative repetitive structure comprising two hemispherical grains in contact, as illustrated in Figure 3. Once stress is applied, the quartz aggregates may consolidate to more dense packing, i.e., lower porosity due to grain rearrangement. However, we do not take into account the effect of mechanical consolidation, of grain crushing at Hertzian contacts, and attendant influences on reactive surface area and mass diffusion coefficients. Porosity decrease is assumed to result only as a result of pressure solution process.

[18] Upon initiation of the deformation process, the grain-to-grain contact is so small that there is a strong enhancement of the local stress. These stress concentrations may be further enhanced by the presence of local short-wavelength irregularities at the grain contacts that will be rapidly removed by pressure solution to produce the idealized geometry assumed in Figure 1. Pressure solution will proceed rapidly from this initial condition, registered as a rapid initial decrease in porosity with time. As dissolution proceeds, the intergranular contact area increases, and the intergranular stress concomitantly decreases. Ultimately, dissolution and the associated compaction will cease as intergranular stresses approach the critical stress that implies equilibrium. The resulting quartz solute is suspended in the pore fluid and/or precipitated on the free surfaces by successive layers of a solid thin film (see Figure 3 and more details are provided in Appendix A). Note that in a closed system the amount of quartz solute transported from the intergranular contact must balance the sum of the component amounts suspended in the pore fluid and precipitated on the peripheries of grains. Where advective flow through the pore structure is significant, the quartz mass removed from the representative elemental volume per unit
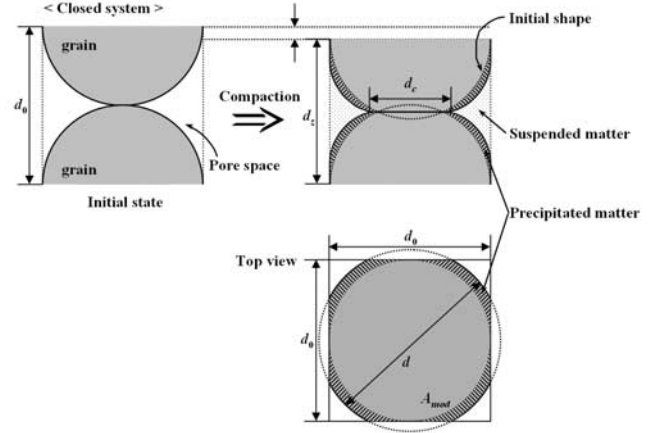

Figure 3. Proposed geometric model of grain-to-grain contact. Initially, two hemispheres, of diameter, d_0, are in contact. As compaction proceeds ($d_z < d_0$), the diameter of the contact area, d_c, increases, and the quartz removed from the grain-to-grain contact is suspended in the pore fluid and/or precipitated on the free faces. Grain geometries become truncated spheres of diameter, d, of cross-sectional area, A_{mod}.

time is accommodated as the product of volume flux and average aqueous concentration.

2.6. Ensemble System

[19] An important component of this model is the ability to concurrently calculate the solute concentrations that develop both at the interface between grains and within the pore fluid. Importantly, this relaxes the requirement that the system must be closed, as the mass removed by advective fluxes may be straightforwardly evaluated. To achieve this, the following numerical technique is adopted.

[20] As shown in Figure 4, the system is divided into two elements with each element representative of one half of the pore space, i.e., $V_p/2$. Assuming that elements 1 and 2 are only controlled by diffusion and precipitation processes, respectively, each element is defined by

$$\left\{ \begin{array}{c} q_1 \\ q_2 \end{array} \right\}_\tau = \frac{2\pi\varpi D_b}{\ln(d_c/2a)} \begin{bmatrix} 1 & -1 \\ -1 & 1 \end{bmatrix} \left\{ \begin{array}{c} C_1 \\ C_2 \end{array} \right\}_\tau + \frac{1}{4} \begin{bmatrix} V_p & 0 \\ 0 & V_p \end{bmatrix} \left\{ \begin{array}{c} \dot{C}_1 \\ \dot{C}_2 \end{array} \right\}_\tau ,$$
$$(18)$$

$$\left\{ \begin{array}{c} q_2 \\ q_3 \end{array} \right\}_\tau = V_p \frac{A}{M} k_- \begin{bmatrix} 1 & -1 \\ -1 & 1 \end{bmatrix} \left\{ \begin{array}{c} C_2 \\ C_3 \end{array} \right\}_\tau + \frac{1}{4} \begin{bmatrix} V_p & 0 \\ 0 & V_p \end{bmatrix} \left\{ \begin{array}{c} \dot{C}_2 \\ \dot{C}_3 \end{array} \right\}_\tau ,$$
$$(19)$$

where q_i and C_i ($i = 1, 2, 3$) are mass fluxes and concentrations at node i. The overscripted dot represents $\dot{C}_i = dC_i/dt$ Considering that $q_1 = dM_{diss}/dt$, $q_2 = q_3 = 0$, and
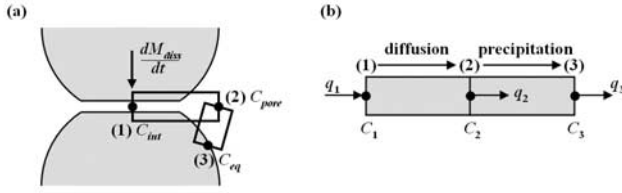
Figure 4. Schematic of discrete technique. (a) Pore space is divided into two elements of axisymmetric form, where each has the volume of $V_p/2$. Nodes 1–3 are placed at the interface of the grain-to-grain contact, pore space, and interface between pore fluid and the free face of grain, respectively. Thus concentrations at nodes 1–3 are regarded as C_{int}, C_{pore}, and C_{eq}, respectively. (b) Elements 1 and 2 are only controlled by diffusion and precipitation, respectively. Each one can be formulated by considering mass conservation.

$C_1 = C_{int}$, $C_2 = C_{pore}$, and $C_3 = C_{eq}$ (Figure 4), equations (18) and (19) can be combined to yield

$$
\left\{ \begin{array}{c} dM_{diss}/dt \\\\ 0 \\\\ 0 \end{array} \right\}_\tau =
\begin{bmatrix} D_1 & -D_1 & 0 \\ -D_1 & D_1 + D_2 & -D_2 \\ 0 & -D_2 & D_2 \end{bmatrix}
\left\{ \begin{array}{c} C_{int} \\\\ C_{pore} \\\\ C_{eq} \end{array} \right\}_\tau
$$
$$
+ \frac{1}{4} \begin{bmatrix} V_p & 0 & 0 \\ 0 & 2V_p & 0 \\ 0 & 0 & V_p \end{bmatrix}
\left\{ \begin{array}{c} \dot{C}_{int} \\\\ \dot{C}_{pore} \\\\ 0 \end{array} \right\}_\tau , \tag{20}
$$

where

$$
D_1 = \frac{2\pi\varpi D_b}{\ln(d_c/2a)}, \qquad D_2 = V_p \frac{A}{M} k_-. \tag{21}
$$

Equation (20) may be integrated in time by applying the implicit method. The temporal derivatives in equation (20) are written at time $\tau = t + \Delta t$, as $\dot{C}_\tau = (C_{t+\Delta t} - C_t)/\Delta t$ and rearranged in terms of concentrations of the interface and pore fluid (first two equations) given by

$$
\left\{ \begin{array}{c} C_{int} \\\\ C_{pore} \end{array} \right\}_{t+\Delta t} =
\begin{bmatrix} D_1 + V_p/4\Delta t & -D_1 \\ -D_1 & D_1 + D_2 + V_p/2\Delta t \end{bmatrix}^{-1}
$$
$$
\cdot \left[\left\{ \begin{array}{c} dM_{diss}/dt \\\\ D_2 C_{eq} \end{array} \right\}_{t+\Delta t} + \frac{1}{4\Delta t} \begin{bmatrix} V_p & 0 \\ 0 & 2V_p \end{bmatrix} \left\{ \begin{array}{c} C_{int} \\\\ C_{pore} \end{array} \right\}_t \right] . \tag{22}
$$

Utilizing this equation, concentrations in the interface and pore fluid can be calculated and updated with time.

2.7. Overall Computational Procedure

[21] The three processes of dissolution, diffusion, and precipitation, coupled with the associated change in geo-metry, are combined to define the progress of porosity reduction with time. The main points of the procedure are as follows.

[22] In the initial condition, a Hertzian contact area is set between the two hemispheres in contact. The representative pore volume is assumed water filled and at an equilibrium concentration of quartz. Thus concentrations of quartz in the interface and pore space are identical to the solubility of quartz, C_{eq}. Once stressed, during time step Δt, dissolution, diffusion, and precipitation mass are simultaneously calculated by equations (12), (15), and (17), respectively. Physically, the dissolved mass evaluated from equation (12) is supplied to the interface, and domain shortening proceeds as this mass passes along the interface by diffusion. Some portion of the dissolved matter is removed from the interface as it exits into the pore fluid, as defined by equation (15). Depending upon the relative concentration differential between the pore fluid solution and the equilibrium concentration, a portion of the mass removed to the pore fluid is deposited to the grain surface (equation (17)), and the geometry of the grain is correspondingly modified (see Appendix A). As a result, the porosity of the system is evaluated and updated. Simultaneously, concentrations in the interface and pore fluid are updated utilizing equation (22). To conduct a consistent calculation until the system reaches an equilibrium state, an iterative procedure is utilized (Figure 5).

3. Comparison With Experimental Measurements

3.1. Matching Laboratory Data

[23] In the previous section, we proposed a mechanistic model to describe the compaction of the porous aggregate. To check its validity, we compare our model with existing experimental measurements [*Elias and Hajash*, 1992].

[24] Compaction experiments have been completed on aggregate samples of rounded quartz sand, of mean grain diameter 180–250 μm, at 150°C [*Elias and Hajash*, 1992]. Changes in porosity and changes in silica concentration in the pore fluid were measured through time to investigate the role of effective stress on silica solubility and compaction rate. In our work we attempt to follow the compaction process by predicting both rates of porosity reduction and evolving concentrations of silica in the pore fluid. To predict response, the appropriate magnitudes of aqueous diffusion coefficient, dissolution rate constant, precipitation rate constant, and the thickness of an interfacial water film (D_b, k_+, k_-, and ω) must be evaluated. Diffusion coefficient, D_b, dissolution rate constant, k_+, and precipitation rate constant, k_-, in equations (12), (15), and (17) all have an Arrhenius-type dependence with temperature given by

$$
D_b = D_0 \exp(-E_D/RT), \tag{23}
$$

$$
k_+ = k_+^0 \exp(-E_{k+}/RT), \tag{24}
$$

$$
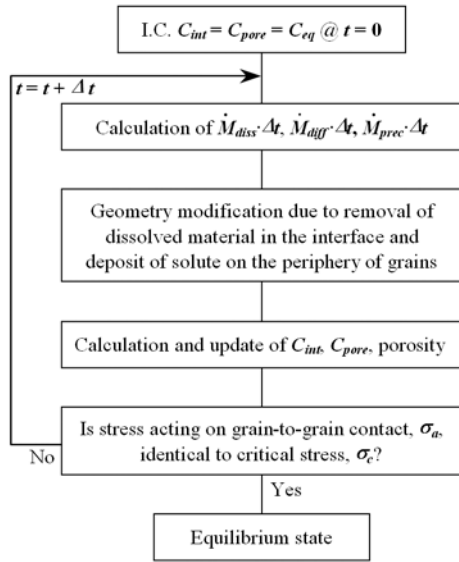k_- = k_-^0 \exp(-E_{k-}/RT). \tag{25}
$$

Figure 5. Iterative procedure to conduct consistent calculations of concentrations at the grain interface, in the pore space and of porosity change with time.

Appropriate magnitudes are selected for these constants defining the temperature dependence as $D_0 = 5.2 \times 10^{-8}$ m^2 s^{-1} and $E_D = 13.5$ kJ mol^{-1} [*Revil*, 1999], $k_+^0 = 1.59$ mol m^2 s^{-1} and $E_{k+} = 71.3$ kJ mol^{-1} [*Dove and Crerar*, 1990], and $k_-^0 = 0.196$ s^{-1} and $E_{k-} = 49.8$ kJ mol^{-1} [*Rimstidt and Barnes*, 1980]. The water film thickness ω in the interface between the grain-to-grain contacts is on the order of 10^{-9} m and dependent on applied stresses [e.g., *Mullis*, 1991; *Heidug*, 1995]. However, this parameter remains ill constrained with no magnitude established by either theoretical or empirical methods, and our calculations are made with an assumed thickness, ω, of 4 nm [e.g., *Revil*, 2001]. Parameters utilized in the calculations are summarized in Table 2. Predicted rates of porosity reduction are shown in Figure 6 together with the data measured within the experiments. To more closely match the porosity and silica concentration histories obtained in the experiments, the principal controlling parameters of diffusion coefficient, D_b, and dissolution and precipitation rate constants (k_+ and k_-) are modified with diffusion coefficient increased by factors of 1.0, 1.0, and 1.5, dissolution rate constant increased by factors of 1.8, 3.0, and 1.0, and precipitation rate constant increased by factors of 13.0, 60.0, and 1.0 for the effective stresses of 69.9, 34.96, and 17.2 MPa, respectively. The predictions of porosity and silica concentration obtained using the modified magnitudes of D_b, k_+, and k_- are in adequate agreement with the actual data, as shown in Figures 6 and 7. In the early period of porosity reduction with time (Figure 6), each experiment has a steeper slope than predictions. This is due to the effect of mechanical consolidation, neglected in the current model. The influence of consolidation can also be recognized from the silica concentration in the pore fluid (Figure 7). Model-derived concentrations increase abruptly to a maximum value after loading, while for the experiments a more gradual rise results. In reality, early

compaction due to rearrangement of grains and load spreading by non-Hertzian contact will reduce average stresses and also reduce the immediate dissolution by pressure solution. Accordingly, silica concentration gradually increases for experiments, while the rapid increase for predictions is observed because the effect of consolidation and non-Hertzian contact is not accommodated.

3.2. Limiting Controls on Deformation

[25] Pressure solution is controlled by the serial processes of dissolution at grain-to-grain contacts, diffusion along the interfacial water film, and then by precipitation from the pore fluid to the free face of grains. If one of these three processes is slower than the other two, it will control the overall deformation (i.e., porosity loss). When compaction proceeds, the reduction in contact stresses due to the increase in contact area may drive a decrease of the dissolution rate. This, in turn, may drive a reduction in diffusive transport due to a lengthening of the transport pathway and of precipitation rate due to reduction in pore wall area available as a deposition site. The evolution of these rates in time, is not uniform, and the dominant mechanism will switch with the duration of compaction process.

[26] The current model has the capability to follow these processes in a natural manner in defining the dominant behavior. Critically, the role of mass concentration is included in the evaluation of response, in accommodating the respective roles of dissolution, diffusion, and precipitation mass flux defined by equations (12), (15), and (17), respectively. Previous laboratory pressure solution experiments have noted the rate-limiting step to be diffusion [*Renard et al.*, 1997], evidenced by the control of a thin water film, in the presence of elevated kinetic rates of dissolution/precipitation in a high effective stress and temperature environment. These observations, under invariant grain geometries, are in agreement with the prediction by *Revil* [2001]. However, our calculations show a transformation from diffusion-limited to dissolution-limited behavior at high effective stresses (69.9 MPa), as illustrated in Figure 8. For the particular stress and temperature conditions, kinetics controls the response to the close of the experimental period ($\sim$200 days). That is, the kinetics of the solid/fluid reaction could be a limiting factor if both the effective stress and temperature are high.

4. Long-Term Behavior

[27] Finally, the processes describing laboratory compaction data may be applied to the long-term prediction of the behavior of geologic processes. Processes controlling the

Table 2. Calculation Parameters to Simulate Experimental Results

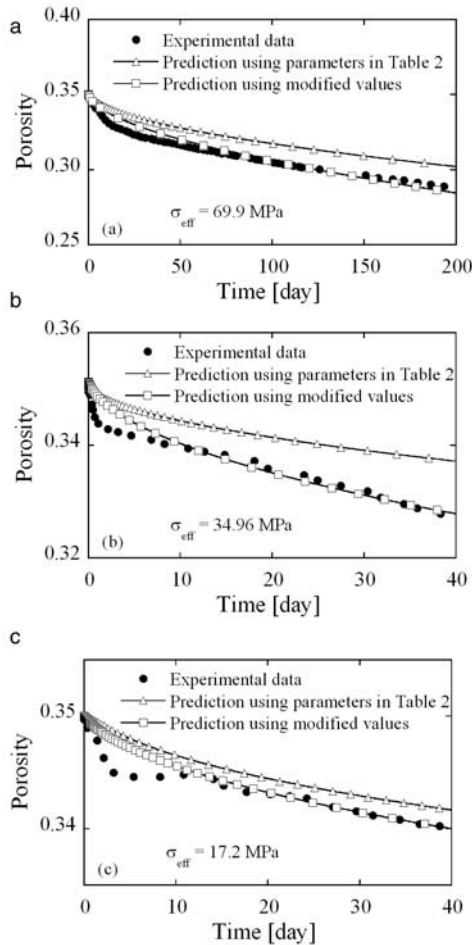| Description	Value
Diameter d, μm	180
Temperature T, °C	150
Effective stress σ_{eff}, MPa	69.9, 34.96, 17.2
Critical stress σ_c, Mpa	73.2
Solubility of quartz C_{eq}, ppm	160
Diffusion Path width ω, nm	4.0
Diffusion coefficient D_b, m^2 s^{-1}	1.12×10^{-9}
Dissolution rate constant k_+, mol m^{-2} s^{-1}	2.51×10^{-9}
Precipitation rate constant k_-, s^{-1}	1.42×10^{-7}

Figure 6. Comparison of porosity reduction with time between the experimental data of *Elias and Hajash* [1992] and the predictions of the model. Open triangles represent the prediction using parameters shown in Table 2, and open squares represent the prediction using modified values with (a) $D_b = 1.0 \times (1.12 \times 10^{-9})$ m^2 s^{-1}, $k_+ = 1.8 \times (2.51 \times 10^{-9})$ mol m^{-2} s^{-1}, and $k_- = 13.0 \times (1.42 \times 10^{-7})$ s^{-1} for $\sigma_{\text{eff}} = 69.9$ MPa, and $T = 150°$C, (b) $D_b = 1.0 \times (1.12 \times 10^{-9})$ m^2 s^{-1}, $k_+ = 3.0 \times (2.51 \times 10^{-9})$ mol m^{-2} s^{-1}, and $k_- = 60.0 \times (1.42 \times 10^{-7})$ s^{-1} for $\sigma_{\text{eff}} = 34.96$ MPa, and $T = 150°$C, and (c) $D_b = 1.5 \times (1.12 \times 10^{-9})$ m^2 s^{-1}, $k_+ = 1.0 \times (2.51 \times 10^{-9})$ mol m^{-2} s^{-1}, and $k_- = 1.0 \times (1.42 \times 10^{-7})$ s^{-1} for $\sigma_{\text{eff}} = 17.2$ MPa and $T = 150°$C.

reduction of porosity toward the ultimate equilibrium state are important in determining the compaction path in sedimentary basins, i.e., the relation between porosity and depth of the sedimentary basin.

[28] To conduct long-term predictions, modified parameters are utilized. Figure 9 represents predictions of porosity and silica concentration obtained with time. These indicate that the porosity and silica concentration decrease in an exponential way with time. Over the short term, silica concentration changes linearly with time, which is in agreement with results obtained by *Dewers and Hajash* [1995] (shown in their Figure 9b). Compaction largely completes within the first decade following the application of effective stress and temperature conditions and reaches

an equilibrium state within a few decades. The ultimate porosity in the equilibrium state is ~0.20, similar to the magnitude predicted by *Revil* [1999].

[29] During diagenesis, fluid expulsion will affect the compactive process by changing effective stresses and in advecting mass to, or from, the compaction site; we consider only the effect of mass advection. To evaluate this effect, our model is extended to represent an open system flushed by a prescribed influent flux of fresh water. An equivalent amount of pore fluid, charged with silica, is concurrently removed. This is accommodated by prescribing an intermediate flux, q_2, in equation (19) that flushes the system defined by

$$q_2 = -C_p \frac{V_p}{t_c}, \tag{26}$$

where t_c represents the time taken to replace one pore volume. For instance, when $t_c = 1$ year, fresh water completely replaces the stagnant pore volume within the period of 1 year. Substituting equation (26) into equation (19), equation (22) is modified as

$$\left\{ \begin{array}{c} C_{\text{int}} \\ \\ C_{\text{pore}} \end{array} \right\}_{t+\Delta t} = \left[\begin{array}{cc} D_1 + V_p/4\Delta t & -D_1 \\ \\ -D_1 & D_1 + D_2 + V_p/2\Delta t \end{array} \right]^{-1}$$

$$\cdot \left[\left\{ \begin{array}{c} dM_{\text{diss}}/dt \\ \\ -C_p V_p/t_c + D_2 C_{\text{eq}} \end{array} \right\}_{t+\Delta t} + \frac{1}{4\Delta t} \left[\begin{array}{cc} V_p & 0 \\ \\ 0 & 2V_p \end{array} \right] \left\{ \begin{array}{c} C_{\text{int}} \\ \\ C_{\text{pore}} \end{array} \right\}_t \right], \tag{27}$$

where

$$D_1 = \frac{2\pi\varpi D_b}{\ln(d_c/2a)}, \qquad D_2 = V_p \frac{A}{M} k_-. \tag{28}$$

Figure 10 shows predictions of porosity, strain (domain shortening is taken as positive in sign), and silica concentration obtained with time for the closed system and the open system with t_c, of 10 days and 1 day. The ultimate porosity retained at the equilibrium state increases with an increase in the advective flux of fresh water. This results from the reduction in silica available to be precipitated on the pore wall, as it is removed by advection. The selected flushing rates, on the order of days, are very large and indicate the unlikely control on compaction by advective fluxes (Figure 10a), although there is a measurable effect. Conversely, the predicted evolution of strain is invariant with advective flux, indicating that for effective stresses of 35 MPa and a temperature of 150°C, the process is dissolution limited, except in the initial stages when diffusion controls the deformation. If the process was controlled either by diffusion or by the kinetics of precipitation, both strain rates and ultimate strain would increase with advective flux. As in the experimental results of Figure 7, mass concentrations initially build as solute
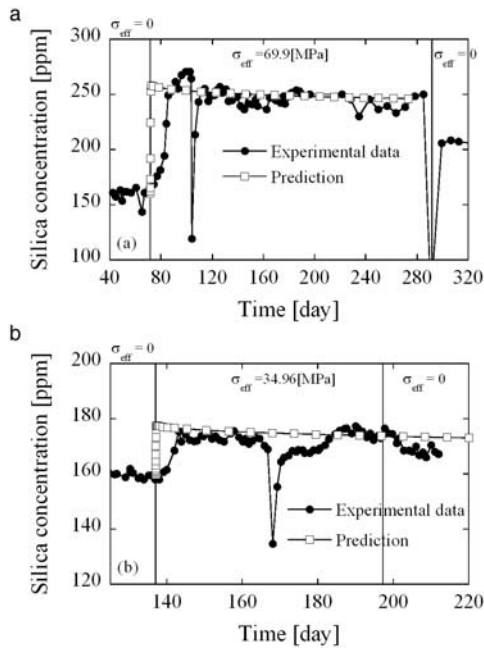
Figure 7. Comparison of silica concentration in the pore fluid between the experimental data of *Elias and Hajash* [1992] and the predictions of the model. (a) For σ_{eff} = 69.9 MPa and T = 150°C, open squares represent the prediction using modified values of $D_b = 1.0 \times (1.12 \times 10^{-9})$ $m^2 s^{-1}$, $k_+ = 1.8 \times (2.51 \times 10^{-9})$ mol m^{-2} s^{-1}, and $k_- = 13.0 \times (1.42 \times 10^{-7})$ s^{-1}. (b) For σ_{eff} = 34.96 MPa and T = 150°C, open squares represent the prediction using modified values of $D_b = 1.0 \times (1.12 \times 10^{-9})$ $m^2 s^{-1}$, $k_+ = 3.0 \times (2.51 \times 10^{-9})$ mol m^{-2} s^{-1}, and $k_- = 60.0 \times (1.42 \times 10^{-7})$ s^{-1}.

diffusion to the pore fluid reservoir accumulates and subsequently drop as precipitation becomes the dominant mechanism of mass transfer; this results as diffusion pathway lengths increase as grain interpenetration proceeds. Where the system is closed, the pore concentration
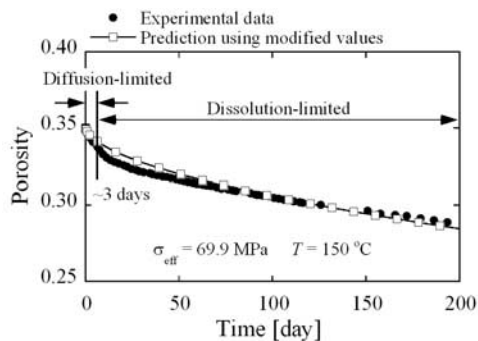

Figure 8. Progressive switch of dominant mechanism during compaction process. Open squares represent the prediction using modified values, with $D_b = 1.0 \times (1.12 \times 10^{-9})$ $m^2 s^{-1}$, $k_+ = 1.8 \times (2.51 \times 10^{-9})$ mol m^{-2} s^{-1}, and $k_- = 13.0 \times (1.42 \times 10^{-7})$ s^{-1} for σ_{eff} = 69.9 MPa and T = 150°C. The predictive result shows that a transformation from diffusion-limited to dissolution-limited behavior occurs around 3 days, and after that dissolution controls the response to the close of the experimental period.

asymptotes to the equilibrium concentration for a temperature of 150°C, as illustrated in Figure 10c. Where the system is open and flushed by fresh water, the equilibrium concentration is diluted by the influx, removing potential precipitate but not significantly accelerating the diffusive flux.

[30] A further comparison is conducted by changing the system temperatures (75° and 300°C) to evaluate the temperature dependence of the processes, as shown in Figures 11 and 12. Note that for 75° and 300°C the diffusion coefficient D_b and dissolution/precipitation rate constants (k_+, and k_-) are obtained by equations (23)–(25), respectively, and are modified by the same factors as was done previously, for the system temperature of 150°C (see section 3.1). The critical stresses, σ_c, obtained by equation (1) are 76.92 and 65.64 MPa, and the solubilities of quartz for 75° and 300°C are obtained as [*Fournier and Potter*, 1982] ~30 and ~1400 ppm, respectively. These parameters are summarized in Table 3. Figures 10–12 indicate that the compaction by pressure solution both proceeds faster and reaches equilibrium more quickly, with an increase in temperature. This is because all three serial processes (i.e., dissolution, diffusion, and precipitation) become more active (see D_b, k_+, and k_- in Tables 2 and 3). Uniformly, the ultimate porosity decreases with an increase in temperature, as the critical stress, σ_c, decreases with increased temperature: a larger grain-to-grain contact area is required for the equilibrium condition at elevated temperatures. As advective flux increases, the change in porosity is reduced
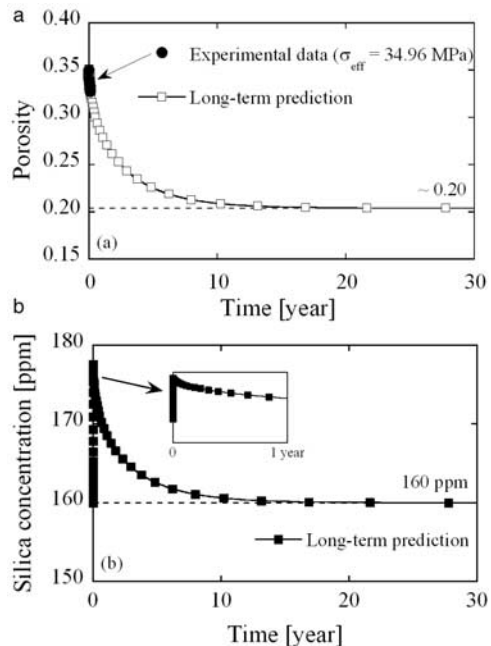

Figure 9. Prediction of long-term compaction behavior for σ_{eff} = 34.96 MPa and T = 150°C. The prediction is conducted utilizing modified values of $D_b = 1.0 \times (1.12 \times 10^{-9})$ $m^2 s^{-1}$, $k_+ = 3.0 \times (2.51 \times 10^{-9})$ mol m^{-2} s^{-1}, and $k_- = 60.0 \times (1.42 \times 10^{-7})$ s^{-1}. (a) Porosity reduction with time. The ultimate porosity approaches ~0.20 when the equilibrium state is reached. (b) Silica concentration changes with time. The concentration approaches silica solubility in the equilibrium state.
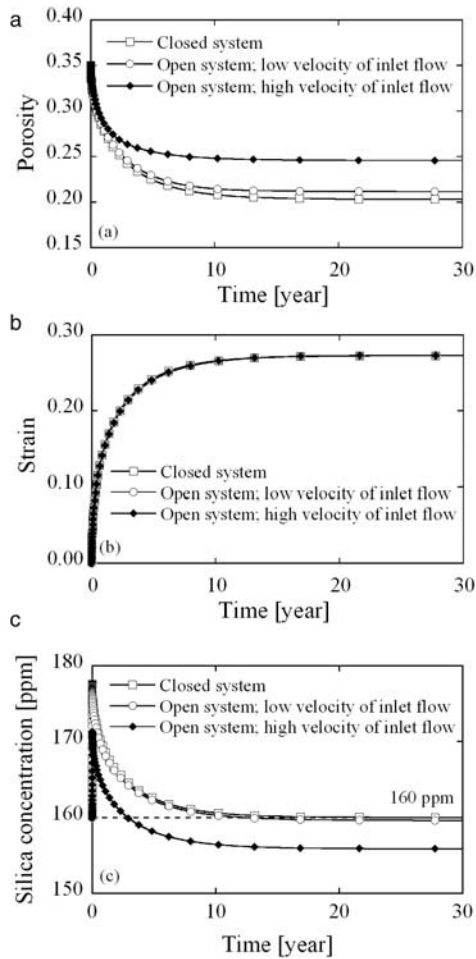
Figure 10. Comparison between closed and open system on long-term compaction behavior for σ_{eff} = 34.96 MPa and T = 150°C. Predictions are conducted utilizing modified values of D_b = 1.0 × (1.12 × 10^{-9}) m^2 s^{-1}, k_+ = 3.0 × (2.51 × 10^{-9}) mol m^{-2} s^{-1}, and k_- = 60.0 × (1.42 × 10^{-7}) s^{-1}. Calculations of open system for low and high velocities of inlet flow are made with t_c = 10 days and 1 day, respectively. (a) Porosity reduction with time. (b) Strain increase with time. (c) Silica concentration change with time.

for the precipitation-controlled conditions, as the excess mass is advected from the system and is unavailable to reduce porosity through grain-face precipitation. In the three cases represented, the late-time behavior is dominated by precipitation, and the flushing by pore fluids at temperatures from 75° to 300°C has little influence on the evolving strain, despite a significant effect on the progress of ultimate steady porosity magnitudes. The compaction processes that take a 1000 years to complete at 75°C takes a fraction of a year at 300°C, as anticipated from the Arrhenius dependence. Likewise, at low temperatures, the supply of mass by diffusion is sufficiently slow that flushing of the pore fluid has the greatest impact in diluting pore fluid concentrations.

[31] Finally, the effect of flushing by pore fluids on the progress of permeability reduction in the aggregate may also be defined. Permeability of the granular aggregate is strongly correlated to the porosity of the media, with the

simplest representative model comprising a capillary tube model [*Bear*, 1972]. Permeability may be related to mean capillary diameter, δ, as

$$k = \frac{n\delta^2}{96},$$ (29)

where k, n, and δ are permeability and porosity of the aggregate, and diameter of the capillary tubes, respectively. Using the grain diameter, d_0, which is equivalent to the domain width (see Figure 3), the pore volume, V_p, is expressed as V_p = $(\pi/4)\delta^2 d_0$, and therefore equation (29) may be rearranged as

$$k = \frac{nV_p}{24\pi d_0}.$$ (30)

Figure 13 shows predictions of permeability obtained with time for three different temperatures and for the closed
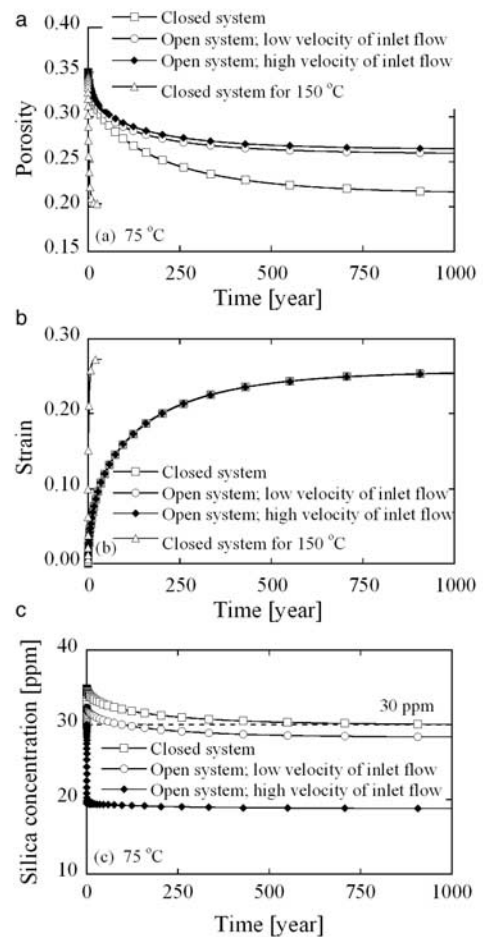

Figure 11. Comparison between closed and open system on long-term compaction behavior for σ_{eff} = 34.96 MPa and T = 75°C. Predictions are conducted utilizing modified values of D_b = 1.0 × (4.90 × 10^{-10}) m^2 s^{-1}, k_+ = 3.0 × (3.19 × 10^{-11}) mol m^{-2} s^{-1}, and k_- = 60.0 × (6.61 × 10^{-9}) s^{-1}. Calculations of open system for low and high velocities of inlet flow are made with t_c = 10 days and 1 day, respectively. (a) Porosity reduction with time. (b) Strain increase with time. (c) Silica concentration change with time.
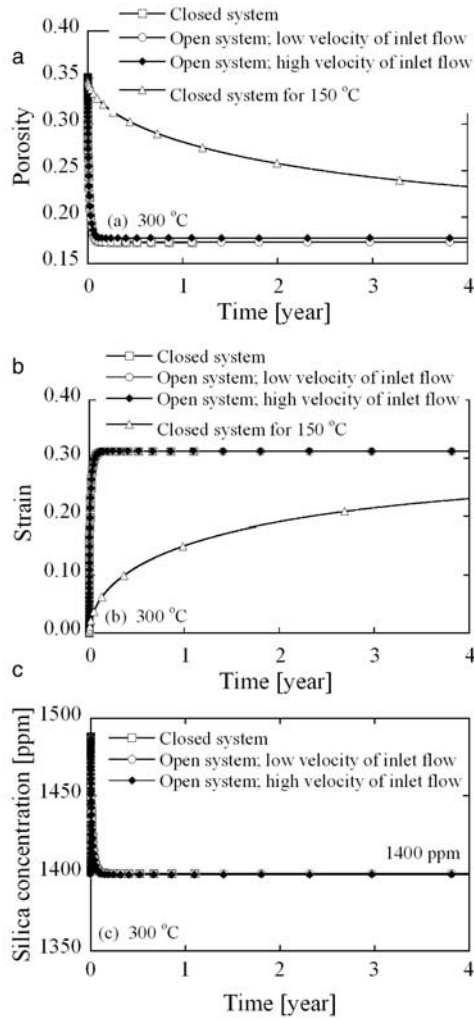
Figure 12. Comparison between closed and open system on long-term compaction behavior for σ_{eff} = 34.96 MPa and T = 300°C. Predictions are conducted utilizing modified values of D_b = 1.0 × (3.06 × 10^{-9}) m^2 s^{-1}, k_+ = 3.0 × (5.05 × 10^{-7}) mol m^{-2} s^{-1}, and k_- = 60.0 × (5.67 × 10^{-6}) s^{-1}. Calculations of open system for low and high velocities of inlet flow are made with t_c = 10 days and 1 day, respectively. (a) Porosity reduction with time. (b) Strain increase with time. (c) Silica concentration change with time.

system and the open system with t_c, of 10 days and 1 day. As expected, permeability decreases with the same tendency as porosity. Increasing the advective flux reduces the change in permeability and shows significant effects at 75° and 150°C, while it has less effect at 300°C. This is because the additional mass, transported into the pore fluid, is rapidly

precipitated onto the pore walls, due to the high-precipitation rate constant, k_-, that acts at 300°C.

5. Conclusions

[32] A mechanistic model is proposed to describe the compaction of porous aggregates that incorporates the important effects of grain interpenetration that accompany the redistribution of mass due to the three serial processes of dissolution, diffusion, and precipitation. The incorporation of these processes, at a micromechanical level, allows the compaction of porous aggregates to develop in a natural manner and the dominant process to develop naturally, at any particular effective stress or temperature regime. The dominant compaction rate-limiting process may switch during the progress of compaction, as the local grain-to-grain contact geometry is modified with interpenetration. As interpenetration occurs, diffusive transport pathways are lengthened, and the rate of mass transfer to the water-filled pore is reduced.

[33] Although relatively simple, the model is capable of representing the compaction process, including defining the important contribution of mass to the evolving pore fluid mass concentration. This specific attribute enables differences in the compaction behavior of both hydraulically closed and open systems to evolve naturally. For closed systems, porosity reduction increases, in both rate and ultimate magnitude as temperature of the system increases; the process of compaction resulting from grain interpenetration that may operate over many centuries at 75°C are shown to take but a fraction of a year at 300°C. For this range of temperatures, the effect of hydraulic circulation is to reduce the ultimate diminution of porosity, as aqueous precipitates are advected from the system but with negligible effect on evolving compaction strains. This is apparent even for unreasonably high replenishment at rates on the order of 0.1–1 pore volumes per day. The diminution of concentrations of pore fluids by flushing is greatest where diffusive transport to the pore fluid is smallest, at low temperatures. The asymptotic porosity is controlled by the magnitudes of the heat and temperature of fusion of quartz, the ambient temperature, and the form of packing of the aggregate. The rate that this asymptotic porosity is attained is controlled by temperature and stress magnitudes. For temperatures in the range 75°–300°C and stresses on the order of 35 MPa considered here, the process is dissolution controlled. Temperature exerts a dominant influence on compaction rate due to the exponential form of the Arrhenius-type dependence of dissolution rate on temperature. This thermal control is much stronger than that of the stress level.

[34] In this work the long-term compaction of loose aggregates is addressed, without consideration of the

Table 3. Calculation Parameters to Simulate Long-Term Behavior for Open System at 75° and 300°C

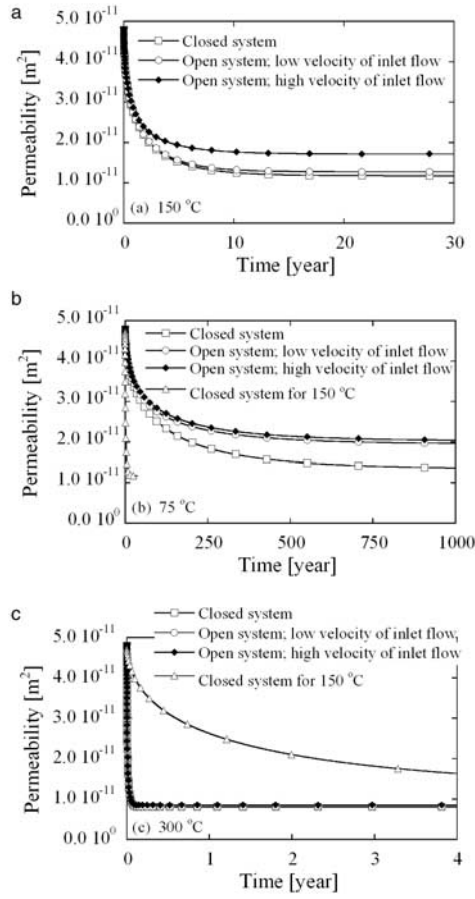| Temperature T, °C	Diffusion Coefficient D_b, m^2 s^{-1}	Dissolution Rate Constant k_+, mol m^{-2} s^{-1}	Precipitation Rate Constant k_-, s^{-1}	Critical Stress σ_c, MPa	Solubility of Quartz C_{eq}, ppm
75	4.90 × 10^{-10}	3.19 × 10^{-11}	6.61 × 10^{-9}	76.92	∼30
300	3.06 × 10^{-9}	5.05 × 10^{-7}	5.67 × 10^{-6}	65.64	∼1400

Figure 13. Evolution of permeability reduction in closed and open system for σ_{eff} = 34.96 MPa. Predictions are conducted utilizing modified values of rate constants identified in Tables 2 and 3. Calculations for the open system are for both low and high velocities of inlet flow and are made with t_c = 10 days and 1 day, respectively. (a) T = 150°C. (b) T = 75°C. (c) T = 300°C.

strength gain anticipated as interpenetrated grain boundaries cement. These considerations are important in considering strength gain in reservoir rocks and the development of seals and strength in active faults [e.g., *Bos et al.*, 2000; *Kanagawa et al.*, 2000], where fault healing may be controlled by processes of pressure solution. In particular, *Tadokoro and Ando* [2002] reported the rapid fault healing that completed within 33 months after the earthquake. This rate is consistent with observations of pressure-solution-driven compaction at the moderate temperatures addressed in this work. This work provides a mechanistic framework to define this likely strength gain, where the system may be either closed or open, and thereby achieve a more realistic understanding of fault healing and of nucleation and recurrence of earthquakes.

Appendix A: Grain Interpenetration

[35] The solid quartz volume, V_s, in the representative elementary volume, as shown in Figure 3, is obtained by subtracting from the volume of a sphere of diameter, d, the sums of the volumes truncated between the hemispheres and

the rectangular domain, and between the contacts of two hemispheres given by

$$V_s = -\frac{\pi}{3}d^3 + \pi d_z\left(\frac{d^2}{4} - \frac{d_z^2}{12}\right) + \pi d_0\left(\frac{d^2}{2} - \frac{d_0^2}{6}\right), \quad \text{(A1)}$$

where d_z and d_0 are the domain height and the initial grain diameter, respectively. In particular, the volume truncated by the two hemispheres in contact, V_{rem}, is given by

$$V_{\text{rem}} = \frac{\pi}{8}\left(\frac{d_z^3}{3} - d_0^2 d_z + \frac{2}{3}d_0^3\right). \quad \text{(A2)}$$

In a closed system the volume of the quartz grain must balance the initial volume of the grain minus the amount suspended in the pore fluid, and the solid quartz volume, V_s, is also expressed as

$$V_s = \frac{\pi}{6}d_0^3 - \frac{1}{\rho_g}\sum\left(\left(\frac{dM_{\text{diff}}}{dt} - \frac{dM_{\text{prec}}}{dt}\right)\Delta t\right), \quad \text{(A3)}$$

where the summation is completed over time, to determine the cumulative volume of the solid removed from the grain. Since the domain shortening proceeds as the mass dissolved passes along the interface by diffusion, the volume truncated by the two hemispheres in contact is given by

$$V_{\text{rem}} = \frac{1}{\rho_g}\sum\left(\frac{dM_{\text{diff}}}{dt}\Delta t\right). \quad \text{(A4)}$$

From equations (A1)–(A4) we can obtain the diameter, d, of the modified sphere and the domain height, d_z. Then using these values, the porosity, ϕ, the cross-sectional area of the modified sphere, A_{mod}, and the diameter of contact area, d_c, are calculated as

$$\phi = 1 - \frac{V_s}{d_0^2 d_z}, \quad \text{(A5)}$$

$$A_{\text{mod}} = \frac{\pi}{4}d^2 - d^2\arccos\left(\frac{d_0}{d}\right) + d_0\sqrt{d^2 - d_0^2}, \quad \text{(A6)}$$

$$d_c = \sqrt{d_0^2 - d_z^2} + (d - d_0). \quad \text{(A7)}$$

[36] For a uniaxial compaction, the force applied at the quartz aggregate balances the force applied at the contact area, and the stress applied at the contact area, σ_a, is obtained as

$$\sigma_{\text{eff}} A_{\text{mod}} = \sigma_a \frac{\pi}{4}d_c^2, \quad \text{(A8)}$$

$$\sigma_a = \sigma_{\text{eff}} \frac{A_{\text{mod}}}{\frac{\pi}{4}d_c^2}. \quad \text{(A9)}$$

Through this process, the grain geometry is modified at each time step, Δt, and the porosity is updated until the

system reaches an equilibrium state when the stress applied at contact area, σ_a, becomes equivalent to the critical stress, σ_c.

References

Bear, J., *Dynamics of Fluids in Porous Media*, pp. 162–165, Dover, Mineola, N. Y., 1972.

Bird, G., J. Boon, and T. Stone, Silica transport during steam injection into oil sands, 1, Dissolution and precipitation kinetics of quartz: New results and review of existing data, *Chem. Geol.*, *54*, 69–80, 1986.

Bos, B., C. J. Peach, and C. J. Spiers, Slip behavior of simulated gouge-bearing faults under conditions favoring pressure solution, *J. Geophys. Res.*, *105*, 16,699–16,717, 2000.

Canals, M., and J. D. Meunier, A model for porosity reduction in quartzite reservoirs by quartz cementation, *Geochim. Cosmochim. Acta*, *59*, 699–709, 1995.

Coble, R. L., A model for boundary diffusion controlled creep in polycrystalline materials, *J. Appl. Phys.*, *34*, 1679–1682, 1963.

Dewers, T., and A. Hajash, Rate laws for water-assisted compaction and stress-induced water-rock interaction in sandstones, *J. Geophys. Res.*, *100*, 13,093–13,112, 1995.

Dewers, T., and P. Ortoleva, A coupled reaction/transport/mechanical model for intergranular pressure solution, stylolites, and differential compaction and cementation in clean sandstones, *Geochim. Cosmochim. Acta*, *54*, 1609–1625, 1990.

Dove, P. M., and D. A. Crerar, Kinetics of quartz dissolution in electrolyte solutions using a hydrothermal mixed flow reactor, *Geochim. Cosmochim. Acta*, *54*, 955–969, 1990.

Elias, B. P., and A. Hajash, Change in quartz solubility and porosity change due to effective stress: An experimental investigation of pressure solution, *Geology*, *20*, 451–454, 1992.

Engelder, T., A natural example of the simultaneous operation of free-face dissolution and pressure solution, *Geochim. Cosmochim. Acta*, *46*, 69–74, 1981.

Fournier, R. O., and R. W. Potter II, An equation correlating the solubility of quartz in water from 25°C to 900°C at pressure up to 10,000 bars, *Geochim. Cosmochim. Acta*, *46*, 1969–1973, 1982.

Heidug, W. K., Intergranular solid-fluid phase transformations under stress: The effect of surface forces, *J. Geophys. Res.*, *100*, 5931–5940, 1995.

Kanagawa, K., S. F. Cox, and S. Zhang, Effects of dissolution-precipitation processes on the strength and mechanical behavior of quartz gouge at high-temperature hydrothermal conditions, *J. Geophys. Res.*, *105*, 11,115–11,126, 2000.

Lehner, F. K., A model for intergranular pressure solution in open systems, *Tectonophysics*, *245*, 153–170, 1995.

Mullis, A. M., The role of silica precipitation kinetics in determining the rate of quartz pressure solution, *J. Geophys. Res.*, *96*, 10,007–10,013, 1991.

Palciauskas, V. V., and P. A. Domenico, Fluid pressures in deforming porous rocks, *Water Resour. Res.*, *32*, 3041–3049, 1996.

Paterson, M. S., A theory for granular flow accommodated by material transfer via an intergranular fluid, *Tectonophysics*, *245*, 135–151, 1995.

Ragnarsdóttir, K. V., and J. V. Walther, Pressure sensitive "silica geothermometer" determined from quartz solubility experiments at 250°C, *Geochim. Cosmochim. Acta*, *47*, 941–946, 1983.

Raj, R., Creep in polycrystalline aggregates by matter transport through a liquid phase, *J. Geophys. Res.*, *87*, 4731–4739, 1982.

Renard, F., P. Ortoleva, and J. P. Gratier, Pressure solution in sandstones: Influence of clays and dependence on temperature and stress, *Tectonophysics*, *280*, 257–266, 1997.

Revil, A., Pervasive pressure-solution transfer: A poro-visco-plastic model, *Geophys. Res. Lett.*, *26*, 255–258, 1999.

Revil, A., Pervasive pressure solution transfer in a quartz sand, *J. Geophys. Res.*, *106*, 8665–8686, 2001.

Rimstidt, J. D., and H. L. Barnes, The kinetics of silica-water reactions, *Geochim. Cosmochim. Acta*, *44*, 1683–1699, 1980.

Robin, P.-Y. F., Pressure solution at grain to grain contacts, *Geochim. Cosmochim. Acta*, *42*, 1383–1389, 1978.

Rutter, E. H., The kinetics of rock deformation by pressure solution, *Philos. Trans. R. Soc. London, Ser. A*, *283*, 203–219, 1976.

Shimizu, I., Kinetics of pressure solution creep in quartz: Theoretical considerations, *Tectonophysics*, *245*, 121–134, 1995.

Stephenson, L. P., W. J. Plumley, and V. V. Palciauskas, A model for sandstone compaction by grain interpenetration, *J. Sediment. Petrol.*, *62*, 11–22, 1992.

Tada, R., and R. Siever, Experimental knife-edge pressure solution of halite, *Geochim. Cosmochim. Acta*, *50*, 29–36, 1986.

Tada, R., R. Maliva, and R. Siever, Rate laws for water-assisted compaction and stress-induced water-rock interaction in sandstones, *Geochim. Cosmochim. Acta*, *51*, 2295–2301, 1987.

Tadokoro, K., and M. Ando, Evidence for rapid fault healing derived from temporal changes in *S* wave splitting, *Geophys. Res. Lett.*, *29*(4), 1047, doi:10.1029/2001GL013644, 2002.

Weyl, P. K., Pressure solution and force of crystallization: A phenomenological theory, *J. Geophys. Res.*, *64*, 2001–2025, 1959.

————————
D. Elsworth, A. Polak, and H. Yasuhara, Department of Energy and Geo-Environmental Engineering, Pennsylvania State University, University Park, PA 16802, USA. (elsworth@psu.edu; abp3@psu.edu; huy103@psu.edu)